Desalination and Water Treatment
www.deswater.com
doi: 10.1080/19443994.2013.859100

53 (2015) 1735–1743
February

Taylor & Francis
Taylor & Francis Group

Membrane fouling properties in a submerged membrane bioreactor for saline wastewater treatment at high ammonium content

Ying An[a], Zhiwei Wang[b,*], Bin Li[b], Zhichao Wu[b], Yifan Zhang[b]

[a]*College of Environmental and Chemical Engineering, Shanghai University of Electric Power, Shanghai 200090, P.R. China*
[b]*State Key Laboratory of Pollution Control and Resource Reuse, College of Environmental Science and Engineering, Tongji University, Shanghai 200092, P.R. China*
Tel./Fax: +86 21 65980400; email: zwwang@tongji.edu.cn

Received 30 May 2013; Accepted 11 October 2013

ABSTRACT

In this study, membrane fouling was characterized in a submerged membrane bioreactor employed for the treatment of saline wastewater containing high ammonium content. Three-dimensional excitation–emission matrix (EEM) fluorescence spectroscopy, scanning electron microscopy (SEM), energy-diffusive X-ray (EDX) analyzer, and atomic force microscopy (AFM) were used to analyze the characteristics of the membrane foulants. The results indicated that the gel layer resistance was the major contributor to the total resistance, which eventually led to a severe loss of permeability. The SEM and AFM analyses showed that a slime gel layer was formed on membrane surfaces, which also had a rough surface morphology. The EEM demonstrated that protein-like substances were dominant in the organic substances with fluorescence characteristics in the gel layer. The examination by EDX demonstrated that Na was the major inorganic elements in the gel layer and that the high valence ions such as Si, Al, and Ca were slightly detectable in the foulants.

Keywords: Ammonium removal; Gel layer; Membrane bioreactor (MBR); Membrane fouling; Saline wastewater

1. Introduction

Wastewater with salinity over 1% is considered to be saline wastewater [1], which can be divided into wastewater discharged from the utilization of seawater, industrial wastewater, and other high-salinity wastewater [2]. The widely used methods for high-salinity wastewater treatment are physicochemical and biological methods. Physicochemical treatment is usually chemically, energetically, and operationally intensive while the biological treatment is an economical and efficient option. However, high salinity in wastewater may inhibit the bacterial activity and affect physicochemical properties of activated sludge, resulting in the changes of surface charge, hydrophobicity, filterability, settlement, and bioflocculation [3].

Membrane bioreactor (MBR) process, which is a promising technology that combines the traditional biological treatment with membrane, has the advantages of small footprint, good effluent quality, and low sludge production [4,5]. With the rapid development of MBR, it has been expanded for high-salinity wastewater treatment besides municipal wastewater treatment. Under the salinity of 0.9–1.3 g/L, about 90

*Corresponding author.

and 95% of chemical oxygen demand (COD) and ammonium were removed, respectively [6]. However, Jang et al. [7] discovered that the increase of salinity from 5 to 20 g/L resulted in the decrease of ammonium removal efficiency from 87 to 46% while there was no obvious influence on the removal efficiency of dissolved organic carbon. Pendashteh et al. [8] observed that the COD removal efficiency was about 86.2% when COD loading rate was 1.12 kg COD/(m^3 d) with hydraulic retention time (HRT) 48 h and total dissolved solids (TDS) 35.0 g/L in a membrane sequencing batch reactor for treating hypersaline wastewater. Besides, Artiga et al. [9] utilized an MBR to treat wastewater streams generated in a fish canning factory during tuna cooking with brine and observed that the removal rate of COD was 92% when the microorganisms adapted to the salinity of 84 g/L after 73-d operation. The intensive researches mentioned above are very helpful for understanding the MBR performance for treatment of saline wastewater; however, the information on membrane fouling behaviors under high salinity is insufficient.

Membrane fouling is one of technical obstacles hindering the application of MBRs [10–12]. Microbes under high salinity might behave very differently compared to those in MBRs for municipal wastewater treatment, which can result in a varied production of extracellular polymeric substances (EPS) and soluble microbial products (SMP). A high salinity can contribute to membrane fouling as well [13], which may increase the gelling potential of microbial products [14]. Therefore, understanding of membrane fouling in MBRs under high salinity is very essential in order to further improve MBR performance.

In this study, a pilot-scale MBR was used to treat wastewater of high salinity (5 g/L Na^+), high ammonium concentration (200 mg/L), and low carbon source concentration (33.7 mg/L). Membrane fouling properties in this MBR were investigated during 130-d operation. Three-dimensional excitation emission matrix (EEM) fluorescence spectroscopy, scanning electron microscopy (SEM), energy-diffusive X-ray (EDX) analyzer, and atomic force microscopy (AFM) were used to analyze membrane fouling properties.

2. Materials and methods

2.1. MBR operation

The MBR system as shown in Fig. 1, which was located at Bailonggang Municipal Wastewater Treatment Plant (WWTP) in Shanghai, China, had an effective volume of 30 L and an average HRT of 20 h. Four flat sheet membrane modules, with the total

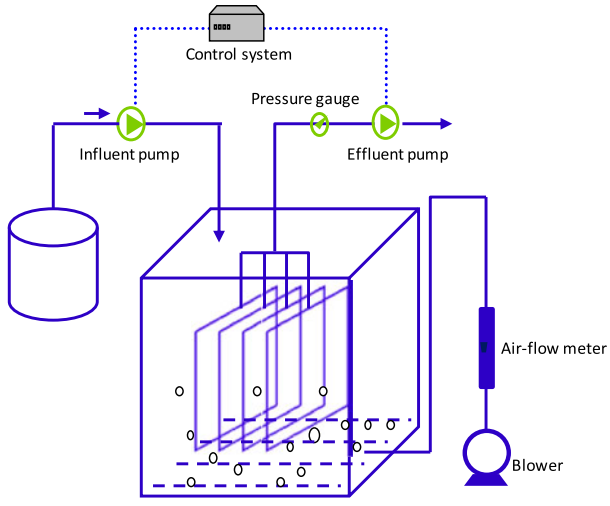

Fig. 1. Flow diagram of the pilot-scale aerobic MBR.

effective filtration area of 0.24 m^2, were vertically submerged in the MBR. The membrane modules, which were made from polyvinylidene fluoride with a mean pore size of 0.2 μm, were supplied by Zizheng Environment Incorporated, Shanghai, China. Aeration was provided in order to supply oxygen demanded for microbes and to produce a cross-flow velocity along the membrane surfaces. A temperature controller was used to maintain the temperature at 25±2℃ in the mixed liquor. During 130-d operation, the dissolved oxygen concentration and pH were kept at 3.4±1.5 and 7.5±0.5 mg/L, respectively. No activated sludge was discharged from the reactor during the experiment.

The influent wastewater used in this experiment was first collected from the secondary sedimentation tank of the WWTP, and then, mixed with sodium bicarbonate and ammonium chloride. The wastewater characteristics are summarized in Table 1. Two peristaltic pumps were utilized to continuously feed the influent and to extract permeate from the

Table 1
Average characteristics of the used wastewater

Items[a]	Concentration
COD (mg/L)	33.7±1.7
NH_3–N (mg/L)	164.4±37.0
NO_2–N (mg/L)	1.9±1.6
TP (mg/L)	0.31±0.11
Na^+ (g/L)	5.0±0.1

[a]Values are given as mean value±standard deviation. The number of measurements (*n*) is 127.

membrane module at a membrane flux of 6 L/(m^2 h), respectively. The trans-membrane pressure (TMP) was measured by a mercury pressure gage. Chemical cleaning (0.5% (v/w) NaClO solution, 24 h duration) would be conducted if TMP was higher than 30 kPa.

2.2. Analytical methods

2.2.1. Membrane foulants collection and pretreatment

The fouled membranes were taken out from the bioreactor at the end of each operation cycle when the TMP reached about 30 kPa, and then, the gel-like layer was carefully scraped from membrane surfaces by a clean plastic sheet [12]. The collected sample was diluted to 500 mL in a beaker and mixed well. The mixed liquor samples could be used for further analysis after filtrating through a membrane with a mean pore size of 0.45 μm [15].

2.2.2. SMP and EPS extraction and analysis

SMP and EPS extractions from the bulk sludge were performed according to the procedures depicted by Wu et al. [16], and then the collected samples were prepared and could be further treated according to the requirements of specific analyses [12].

2.2.3. EEM fluorescence spectra analysis

Fluorescence measurements were conducted using a Horiba Jobin Yvon Fluoromax-4 spectrofluorometer equipped with a 50 W ozone-free Xenon arc lamp and a R928P photomultiplier tube as a detector. The spectrofluorometer can collect the signal in ratio mode with dark offsets using a 5 nm bandpass on the excitation as well as emission monochromators [17]. To obtain fluorescence EEM spectra, excitation wavelengths were incremented from 220 to 600 nm at 5 nm steps, while the emission wavelengths were detected from 220 to 600 nm at same steps. Scan speed was set at 1,200 nm/min, generating an EEM spectrum within 15–17 min. The spectrum of sealed distilled water was recorded as the blank. The software Origin 8.1 (OriginLab Corporation, USA) was employed for handling the EEM data. The EEM spectra were plotted as the elliptical shape of contours. The *X*-axis represents the emission spectra from 220 to 600 nm while the *Y*-axis indicates the excitation wavelength from 220 to 600 nm, and the contour line is shown to express the fluorescence intensity at an interval of 5.

2.2.4. SEM-EDX analysis

For SEM analysis, the flat sheet membrane covered with gel-like layer was removed from the MBR after one operation cycle, and then, a piece of the membrane was cut from the middle of the module. The membrane sample was dried at room temperature and fixed with 2.0% glutaraldehyde in 0.1 M phosphate buffer at pH 7.2, and then dehydrated with ethanol and coated with aurum–platinum alloy with coating depth 10 nm and observed using the SEM (Model XL-30, Philips, the Netherlands). The EDX analyzer (Phoenix, EDAX Incorporated, USA) was also employed to characterize the inorganic components of the gel layer.

2.2.5. AFM analysis

AFM analysis was carried out to investigate the surface morphology and topography of the virgin and fouled membranes, which were dried at ambient temperature of 20±1℃. The images, which were fixed on a slide glass and obtained in the range 5 μm × 5 μm, were observed using the electrochemical scanning probe microscopy (ECSPM: Pico-SPM, Molecular Imaging Co., USA).

2.2.6. Resistance analysis

The hydraulic resistance was calculated using the resistance-in-series model [13,16]:

$$R_t + R_m + R_c + R_f = \frac{TMP}{\mu J} \times 3,600 \quad (1)$$

where R_t is the total membrane resistance (m^{-1}), R_m the intrinsic membrane resistance (m^{-1}), R_c the gel layer resistance (m^{-1}), R_f the fouling resistance due to irreversible adsorption and pore plugging, J the instantaneous flux ($m^3/(m^2\ h)$), TMP the TMP (Pa), and μ the dynamic viscosity of permeate water (Pa s).

In this study, R_m was calculated by filtrating deionized water with new membrane module. At the end of operation cycle, R_t was calculated by flux and TMP. After that, the membrane surface gel layer was carefully removed from membrane surfaces by a sponge. R_m + R_f was obtained by filtrating de-ionized water with this cleaned membrane module. Finally, the value of R_m, R_t, $R_{f,}$ and R_c was obtained separately.

2.2.7. Other item analysis

Chinese NEPA standard methods were used to measure COD, total phosphorus (TP), ammonium

(NH_3–N) and pH in the influent and membrane effluent, and MLSS in the system [18]. DO concentration in the reactor was detected by a dissolved oxygen meter (Model YSI 58, YSI Research Incorporated, OH, USA). Total organic carbon (TOC) was measured by a TOC analyzer (TOC-VcPN, shimadzu, Japan).

3. Results and discussion

3.1. MBR performance

Fig. 2(a) shows the results of ammonium removal with different influent ammonium loading rates (ALR). Feeding was started at a lower ammonium concentration of 62.4±3.4 mg/L at HRT of 20 h (ALR = 0.08±0.01 kg NH_3-N/m^3 d), and the removal efficiency was about 52% on average. Seven days later, the effluent ammonium concentration was decreased to 0.2 mg/L, and the removal efficiency was 99.8%. It showed that 5 g/L Na^+ had no significantly negative effects on the ammonium removal efficiency. According to the report on the effect of salt concentration on MBR performance by Jang et al. [7], the removal efficiency of ammonium was recovered after 30–40 d operation which was much longer than our study. When ALR in the aeration tank was gradually increased to 0.2 kg NH_3–N/(m^3 d), the capability of ammonium removal in the system was not deteriorated. The average effluent ammonium concentration was about 0.9 mg/L, and the average removal efficiency was approximately 99.4%. The influent ammonium was converted into nitrite by ammonium oxidizing bacteria (AOB) and then into nitrate by nitrite oxidizing bacteria (NOB). Aslan et al. reported that as salts added into the feed wastewater were over than 10 g NaCl/L, inhibition effects on the nitrite oxidizing bacteria (NOB) were severer than that on the AOB and the NO_2-N/NO_x-N ratio was increased from 0.75 to 0.86 [19]. The same phenomenon was observed in the period of acclimation in our study (Fig. 2(b)). The NO_2-N/NO_x-N ratio was in the range of 0.109–0.964 from 7 d to 24 d, but no significant nitrite accumulation was observed after 24-d operation.

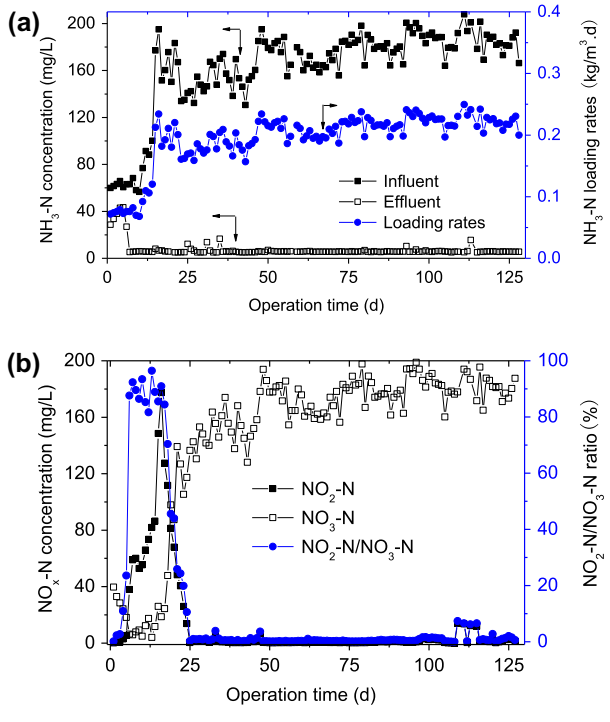

Fig. 2. (a) NH_3–N concentration and loading rates variations during the experiment and (b) effluent concentrations of nitrogen compounds and NO_2-N/NOx-N ratio during the experiment.

For MBR systems, TMP increasing rate is considered as an important factor affecting the membrane filtration performance [20,21]. The changes of TMP over operation time are demonstrated in Fig. 3(a). It can be observed that the TMP increased with operation time as membrane flux was kept at about 6 L/(m^2 h) during the experiment. In Run 1, the TMP increasing rate was 0.9375 kPa/d, higher than that in Run 2 (0.3125 kPa/d). In general, TMP variations could be characterized by a two-step fouling phenomenon, i.e. a long-term slow rise in TMP followed by a rapid increase [12]. However, the two-step fouling phenomenon only occurred in Run 2 while one stage fouling was observed in Run 1. It might be due to the fact that the acclimation period (Run 1) is needed for the microbes to treat saline wastewater. In Fig. 4, it can be observed that the concentration of MLSS in the reactor was gradually decreased during the first 26 d after start-up. High salt concentrations in wastewater can cause cell lysis and death of microbes due to the increase of osmotic pressure, which leads to a decrease of particle diameter and MLSS concentration [7]. After the microbes were adapted to the saline environment, the MLSS concentration started to increase and became stable afterward (Run 2).

To identify the main contributor to membrane fouling, the fractions of membrane resistance were measured and results are displayed in Fig. 3(b). The results showed that intrinsic membrane resistance, internal fouling resistance, and gel layer resistance accounted for 3.1, 3.6, and 93.3% of the total resistance, respectively. This finding indicates that the gel layer resistance was the major contributor to the total resistance and mainly responsible for the TMP increase, which eventually led to a severe loss of permeability [13].

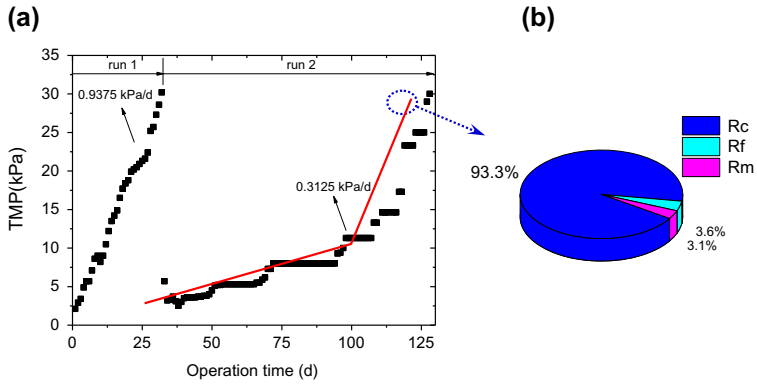

Fig. 3. (a) Variations of TMP during the experiment and (b) resistance distribution of membranes at the end of the operation cycle.

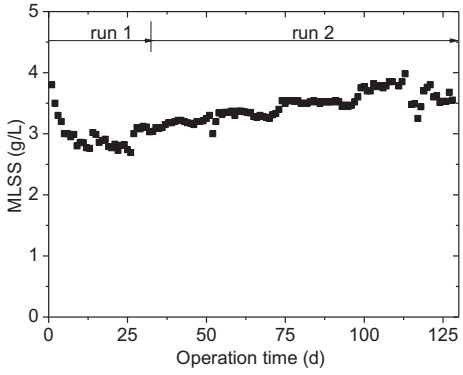

Fig. 4. Changes of MLSS during the experiment.

3.2. EEM fluorescence spectra analysis

EEM spectroscopy has been widely used to characterize the chemical compositions of dissolved organic matter in water and soil [22]. In this study, in order to get more information about the similarities and the differences of the bulk sludge and the gel layer, the EEM analysis was conducted to provide spectral information about the chemical compositions of SMP of the bulk sludge, EPS extracted from the bulk sludge, and SMP of the gel layer. Measurements of EEM fluorescence spectra were carried out in triplicate and similar results were obtained. The representative spectra are therefore shown in Fig. 5.

There are four key fluorescence peaks, Peak A, Peak B, Peak C, and Peak D, observed in these three samples. The excitation and emission boundaries were divided into five regions by Chen et al. to evaluate aromatic protein I-like, aromatic protein II-like, soluble microbial by-product-like, humic acid-like, and fulvic acid-like substances [23]. Peaks A and B were described as the aromatic protein-like substances and tryptophan protein-like substances, respectively [24]. Peak C and Peak D were considered to be the visible fluorescence of humic acid-like substances [25]. As shown in Fig. 5, Peak A was only identified for SMP fraction of the gel layer.

EEM spectra can also be used for quantitative analysis [26]. Fluorescence parameters, such as peak location and maximum fluorescence intensity, were obtained from the EEM fluorescence spectra (listed in Table 2). In this study, three main peaks were observed in SMP spectra and EPS spectra for the bulk sludge, respectively. Compared with the SMP fraction, the locations of Peak B and Peak C in the EPS fraction showed a red shift, while the location of Peak D showed a blue shift. A blue shift is related to a decomposition of condensed aromatic moieties and the breakup of the large molecules into smaller fragments [27], while a red shift is related to the presence of carbonyl containing substituents, hydroxyl, alkoxyl, amino groups, and carboxyl constituents [24]. The intensities of peaks C and D were much higher than that of Peak B for the SMP fraction and much weaker than that of Peak B for the EPS, respectively. It indicates that the visible humic acid-like substances were the main components of the organic matters with fluorescence characteristics in the SMP of bulk sludge. The results also reveal that protein- and SMP-like substances were dominant among fluorescent organic matters in EPS from the bulk sludge [22]. The locations of the three peaks in EPS spectra in this study, at the Ex/Em of 280/345, 355/450, and 250/450 nm, were different from those observed by others authors [24,26,27]. It might be attributed to the fact that the EPS samples were extracted from different origins (saline environment in this study), and thus, the components in EPS were chemically different [22].

Fig. 5(c) shows EEM fluorescence spectra of the SMP extracted from the gel layer. Four main peaks

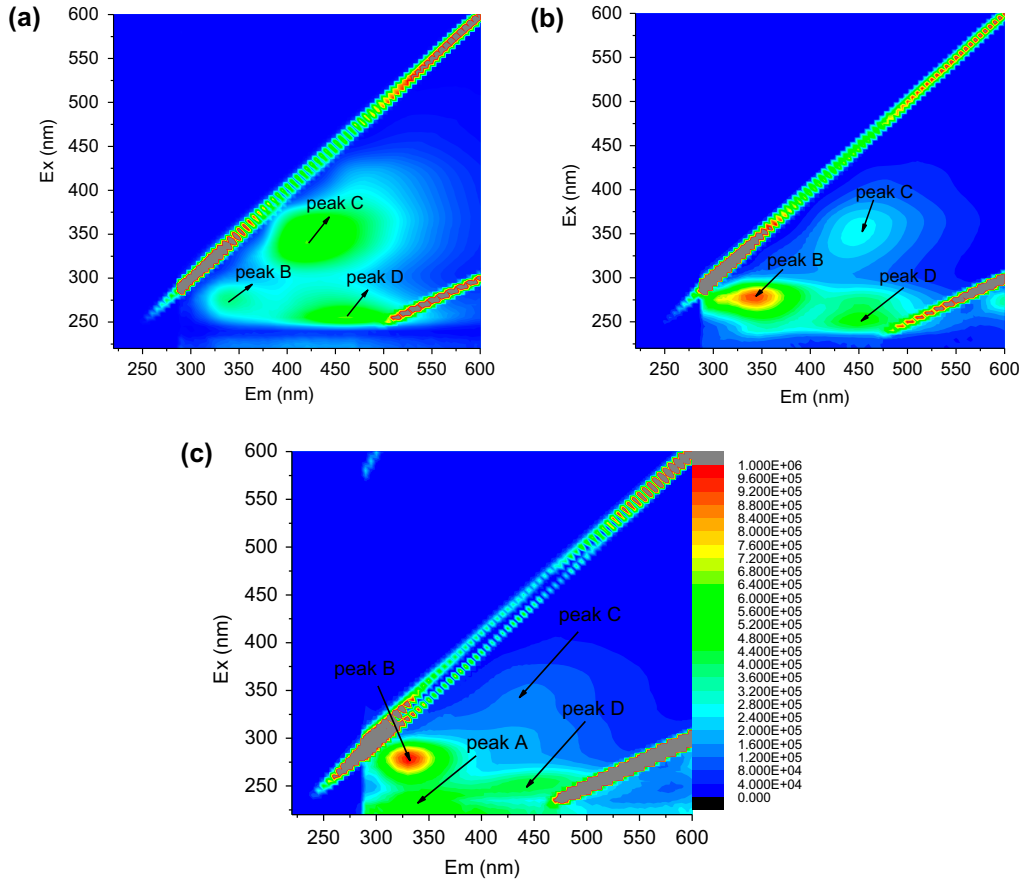

Fig. 5. EEM fluorescence spectra of (a) SMP of bulk sludge, (b) EPS of bulk sludge, and (c) SMP of gel layer.

Table 2
Fluorescence spectral parameters of organic matters

		Peak A		Peak B		Peak C		Peak D	
Organic matters	Samples	Ex/Em	Intensity	Ex/Em	Intensity	Ex/Em	Intensity	Ex/Em	Intensity
SMP	Bulk sludge	ND[a]	ND[a]	275/340	366,489	340/420	642,669	255/465	654,920
EPS	Bulk sludge	ND[a]	ND[a]	280/345	925,986	355/450	260,886	250/450	488,234
SMP	gel layer	230/330	636,892	280/330	987,140	350/445	128,209	250/445	440,743

[a]ND: Not detectable.

could be readily observed from Fig. 5(c). Peak A was located at the Ex/Em of 230/330 nm while Peak B was identified at the Ex/Em of 280/330 nm. Peak C was around the Ex/Em of 350/445 nm while Peak D was identified at the Ex/Em of 250/445 nm. Peak B was predominant in the EEM fluorescence spectra of gel layer in MBR, demonstrating that the gel layer was composed of the protein-like substances. As described in Section 3.1, the contribution of gel layer fouling resistance to total resistance reached 93.3%. Therefore, it can be concluded that protein-like substances rather than humic acid-like substances contributed more to the external gel layer fouling resistance. It could also be seen that the location of Peak B in the EEM fluorescence spectra of gel layer is red-shifted by 5 nm along the excitation axis and blue-shifted by 10 nm along the emission axis in comparison with that of SMP of bulk sludge as listed in Table 2. Meanwhile, the location of Peak B of gel layer was blue-shifted to shorter wavelengths than that of

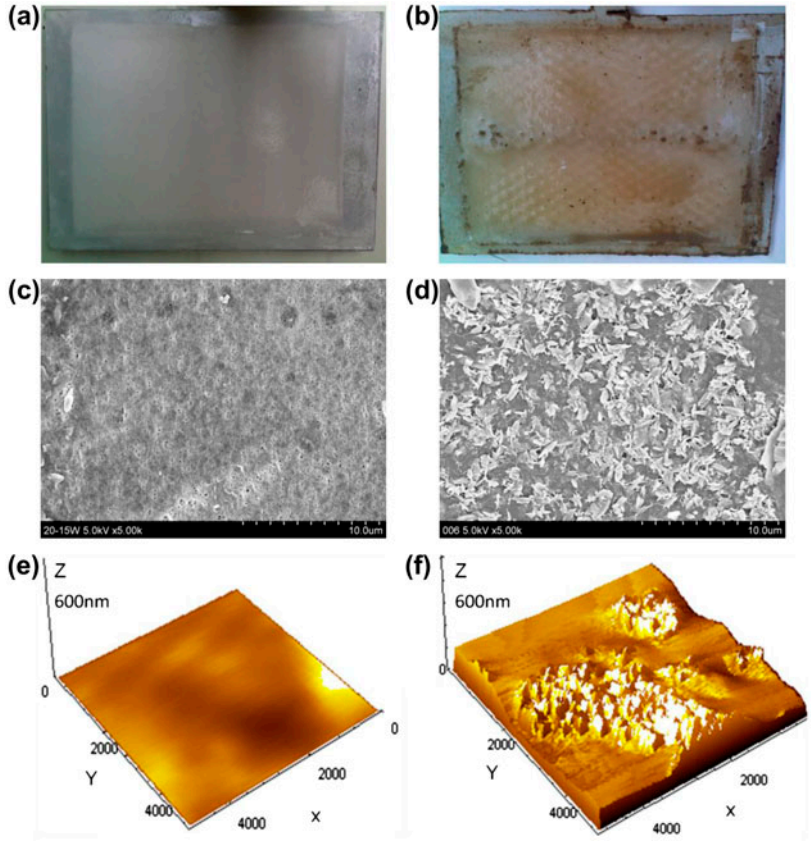

Fig. 6. (a) Photograph of clean membrane module, (b) photograph of fouled membrane module, (c) SEM image of clean membrane, (d) SEM image of fouled membrane, (e) AFM image of clean membrane, and (f) AFM image of fouled membrane.

EPS extracted from bulk sludge. It can be inferred that the structures of protein-like substances represented by Peak B in the gel layer differed from the SMP of bulk sludge and EPS extracted from bulk sludge.

3.3. SEM-EDX analysis

As shown in Fig. 6(b), there was a slime gel layer formed on membrane surfaces compared to Fig. 6(a). It has been reported that a gel layer can be formed in MBRs under sub-critical flux operation because the deposition of sludge flocs is avoided under this operation mode [28]. Therefore, the increase of TMP in this study was mainly due to the formation of the gel layer. SEM images of the cleaned membrane and the fouled membrane are presented in Fig. 6(c) and (d), respectively. Fig. 6(c) shows the new membrane surface, which is free of particles. It demonstrates a network of crests and valleys, which could entrap microbial flocs, macromolecules, and inorganic colloids [13]. The fouled membrane, as shown in Fig. 6(d), appeared to be covered with an uneven and rough gel layer. The results are different from those reported by Wang et al. [24] that a very smooth morphology of gel layer was observed, which needs further investigating.

Table 3
Composition analysis of membrane foulants

Element	C	O	Na	Al	Si	Cl	K	Ca
wt. (%)	43.36	43.87	8.40	0.52	1.86	1.70	0.13	0.17

Table 3 shows SEM-EDX data of chemical elements of the fouling layer. From the elemental analysis, it was found that C and O were the dominant elements of the membrane gel layer, indicating that the organic substances such as polysaccharide and proteins were the main foulants [24]. Compared to the investigations by Wang et al. [12] and An et al. [26], the contents of Na were higher (8.4%), which indicated that a large proportion of the added Na^+ was crystallized on the membrane surface. However, Na was just embedded

in the biopolymers or cells and was not involved in the complex chelation or gelation [24]. Although the relative contents of Al and Ca were very small, these inorganic elements played a significant role in the formation of gel layer, which could bridge the deposited cells and biopolymers and then formed a dense fouling layer when passing through the membranes [12].

3.4. AFM analysis

AFM, which gives topographic images by scanning a sharp tip over a surface, has become an important means of imaging the surface of materials at a resolution up to atomic level [29,30]. AFM images of the new membrane and the fouled membrane are demonstrated in Fig. 6(e) and (f), respectively. The fouled membrane surface had a rough morphology compared to the surface of new membrane. The AFM images exhibit valleys in the new membrane surface (Fig. 6(e)), while the valleys are completely covered with the gel layer on the fouled membrane surfaces.

4. Conclusions

The effluent ammonium concentration of the MBR process under stable condition was around 0.2–0.9 mg/L, indicating that 5 g/L Na^+ had no significant effects on the ammonium removal efficiency when the influent ALR was 0.2 kg NH_3-N/(m^3 d). The fouled membrane surface was covered by a gel layer formed by organic substances and inorganic elements such as Na, Al, K, and Ca, etc. Resistance analysis showed that gel layer resistance accounted for 93.3% of the total resistance. The AFM analysis showed that the new membrane valleys and pore structures were filled with foulants. The visible humic acid-like substances and the protein—and SMP-like substances were the main components of the organic matters with fluorescence characteristics in the SMP and EPS of bulk sludge, respectively. Moreover, the protein-like substances rather than humic acid-like substances contributed more to the gel layer fouling resistance. Further study is needed to investigate the impacts of different salinity and ammonium concentrations on the MBR performance.

Acknowledgement

Financial support of this work by the Science and Technology Commission of Shanghai Municipality (Grant No. 11231200400) is gratefully acknowledged.

References

[1] A.R. Dinçer, F. Kargi, Performance of rotating biological disc system treating saline wastewater, Process Biochem. 36 (2001) 901–906.
[2] X.H. Wen, X.M. Zhan, J.L. Wang, Y. Qian, Review of the biological treatment of salinity wastewater, Environ. Sci. (in Chinese) 20 (1999) 104–106.
[3] E. Reid, X.R. Liu, S.J. Judd, Effect of high salinity on activated sludge characteristics and membrane permeability in an immersed membrane bioreactor, J. Membr. Sci. 283 (2006) 164–171.
[4] Z.W. Wang, Z.C. Wu, Distribution and transformation of molecular weight of organic matters in membrane bioreactor and conventional activated sludge process, Chem. Eng. J. 150 (2009) 396–402.
[5] Z.W. Wang, Z.C. Wu, S.H. Mai, C.F. Yang, X.H. Wang, Y. An, Z. Zhou, Research and applications of membrane bioreactors in China: Progress and prospect, Sep. Purif. Technol. 62 (2008) 249–263.
[6] J.M. Sun, X.H. Wang, R.X. Li, L.F. Dai, W.T. Zhu, Hyperhaline Municipal Wastewater Treatment of a processing zone through Pilot-Scale A/O MBR. Part I: Characteristics of mixture liquor and organics removal, Procedia Environ. Sci. 8 (2011) 773–780.
[7] D. Jang, Y. Hwang, H. Shin, W. Lee, Effects of salinity on the characteristics of biomass and membrane fouling in membrane bioreactors, Biores. Technol. 14 (2013) 50–56.
[8] A.R. Pendashteh, L.C. Abdullah, A. Fakhru'l-Razi, S.S. Madaeni, Z. Zainal Abidin, D.R.A. Biak, Evaluation of membrane bioreactor for hypersaline oily wastewater treatment, Process Saf. Environ. Prot. 90 (2012) 45–55.
[9] P. Artiga, G. García-Toriello, R. Méndez, J.M. Garrido, Use of a hybrid membrane bioreactor for the treatment of saline wastewater from a fish canning factory, Desalination 221 (2008) 518–525.
[10] Z.W. Wang, Z.C. Wu, S.J. Tang, Extracellular polymeric substances (EPS) properties and their effects on membrane fouling in a submerged membrane bioreactor, Water Res. 43 (2009) 2504–2512.
[11] J. Cho, K.G. Song, H. Yun, K.H. Ahn, J.Y. Kim, T.H. Chung, Quantitative analysis of biological effect on membrane fouling in submerged membrane bioreactor, Water Sci. Technol. 51 (2005) 9–18.
[12] Z.W. Wang, Z.C. Wu, X. Yin, L.M. Tian, Membrane fouling in a submerged membrane bioreactor (MBR) under sub-critical flux operation: Membrane foulant and gel layer characterization, J. Membr. Sci. 325 (2008) 238–244.
[13] A.R. Pendashteh, A. Fakhru'l-Razi, S.S. Madaeni, L.C. Abdullah, Z.Z. Abidin, D.R.A. Biak, Membrane foulants characterization in a membrane bioreactor (MBR) treating hypersaline oily wastewater, Chem. Eng. J. 168 (2011) 140–150.
[14] X.M. Wang, T.D. Waite, Impact of gel layer formation on colloid retention in membrane filtration processes, J. Membr. Sci. 325 (2008) 486–494.
[15] Z.C. Wu, X.F. Zhu, Z.W. Wang, Temporal variations of membrane foulants in the process of using flat-sheet membrane for simultaneous thickening and digestion of waste activated sludge, Biores. Technol. 102 (2011) 6863–6869.

[16] Z.C. Wu, Q.Y. Wang, Z.W. Wang, Y.Q. Ma, Q. Zhou, D.H. Yang, Membrane fouling properties under different filtration modes in a submerged membrane bioreactor, Process Biochem. 45 (2010) 1699–1706.
[17] S. Singh, E.J. D'Sa, E.M. Swenson, Chromophoric dissolved organic matter (CDOM) variability in Barataria Basin using excitation-emission matrix (EEM) fluorescence and parallel factor analysis (PARAFAC), Sci. Total Environ. 408 (2010) 3211–3222.
[18] N.E.P.A. Chinese, Water and Wastewater Monitoring Methods. 3rd ed., Chinese Environmental Science Publishing House, Beijing, 1997.
[19] S. Aslan, E. Simsek, Influence of salinity on partial nitrification in a submerged biofilter, Biores. Technol. 118 (2012) 24–29.
[20] B.K. Hwang, W.N. Lee, K.M. Yeon, P.K. Park, C.H. Lee, I.S. Chang, A. Drews, M. Kraume, Correlating TMP increases with microbial characteristics in the bio-cake on the membrane surface in a membrane bioreactor, Environ. Sci. Technol. 42 (2008) 3963–3968.
[21] F.G. Meng, S.R. Chae, A. Drews, M. Kraume, H.S. Shin, F.L. Yang, Recent advances in membrane bioreactors (MBRs): Membrane fouling and membrane material, Water Res. 43 (2009) 1489–1512.
[22] T. Liu, Z.L. Chen, W.Z. Yu, S.J. You, Characterization of organic membrane foulants in a submerged membrane bioreactor with pre-ozonation using three-dimensional excitation-emission matrix fluorescence spectroscopy, Water Res. 45 (2011) 2111–2121.
[23] W. Chen, P. Westerhoff, J.A. Leenheer, K. Booksh, Fluorescence excitation—Emission matrix regional integration to quantify spectra for dissolved organic matter, Environ. Sci. Technol. 37 (2003) 5701–5710.
[24] Q.Y. Wang, Z.W. Wang, Z.C. Wu, J.X. Ma, Z.Y. Jiang, Insights into membrane fouling of submerged membrane bioreactors by characterizing different fouling layers formed on membrane surfaces, Chem. Eng. J. 179 (2012) 169–177.
[25] W.H. Li, G.P. Sheng, X.W. Liu, H.Q. Yu, Characterizing the extracellular and intracellular fluorescent products of activated sludge in a sequencing batch reactor, Water Res. 42 (2008) 3173–3181.
[26] Y. An, Z.W. Wang, Z.C. Wu, D.H. Yang, Q. Zhou, Characterization of membrane foulants in an anaerobic non-woven fabric membrane bioreactor for municipal wastewater treatment, Chem. Eng. J. 155 (2009) 709–715.
[27] Z.W. Wang, Z.C. Wu, S.J. Tang, Characterization of dissolved organic matter in a submerged membrane bioreactor by using three-dimensional excitation and emission matrix fluorescence spectroscopy, Water Res. 43 (2009) 1533–1540.
[28] C.H. Wei, X. Huang, R. Ben Aim, K. Yamamoto, G. Amy, Critical flux and chemical cleaning-in-place during the long-term operation of a pilot-scale submerged membrane bioreactor for municipal wastewater treatment, Water Res. 45 (2011) 863–871.
[29] G.J. Zhang, S.L. Ji, X. Gao, Z.Z. Liu, Adsorptive fouling of extracellular polymeric substances with polymeric ultrafiltration membranes, J. Membr. Sci. 309 (2008) 28–35.
[30] N. Hilal, H. Al-Zoubi, N.A. Darwish, A.W. Mohammad, M. Abu Arabi, A comprehensive review of nanofiltration membranes: Treatment, pretreatment, modelling, and atomic force microscopy, Desalination 170 (2004) 281–308.